UC-413

LBL-26810
Preprint

Lawrence Berkeley Laboratory
UNIVERSITY OF CALIFORNIA

Submitted to Nuclear Physics A

Theory of Nuclear Multifragmentation
II. Post-Transition Dynamics

J.A. López and Jørgen Randrup

November 1989

For Reference

Not to be taken from this room

NUCLEAR SCIENCE DIVISION

LBL-26810
Copy 1
Bldg. 50 Library.

Prepared for the U.S. Department of Energy under Contract Number DE-AC03-76SF00098.

DISCLAIMER

This document was prepared as an account of work sponsored by the United States Government. While this document is believed to contain correct information, neither the United States Government nor any agency thereof, nor the Regents of the University of California, nor any of their employees, makes any warranty, express or implied, or assumes any legal responsibility for the accuracy, completeness, or usefulness of any information, apparatus, product, or process disclosed, or represents that its use would not infringe privately owned rights. Reference herein to any specific commercial product, process, or service by its trade name, trademark, manufacturer, or otherwise, does not necessarily constitute or imply its endorsement, recommendation, or favoring by the United States Government or any agency thereof, or the Regents of the University of California. The views and opinions of authors expressed herein do not necessarily state or reflect those of the United States Government or any agency thereof or the Regents of the University of California.

LBL-26810

Theory of Nuclear Multifragmentation
II. Post-Transition Dynamics*

Jorge A. López† *and Jørgen Randrup*

Nuclear Science Division, Lawrence Berkeley Laboratory
University of California, Berkeley, California 94720

November 22, 1989

Abstract:

Recently expressions were derived for the rate at which a highly excited nucleus breaks up into several interacting prefragments. The present work treats the dynamical evolution of the system subsequent to such a transition. The post-transition system is described as a number of distinct prefragments that experience both conservative and dissipative pairwise interactions, obtained by a suitable generalization of the dynamics governing damped nuclear reactions. The post-transition dynamics has a significant effect on the disassembly process. Most importantly, some prefragments may fuse in the course of the evolution, thus reducing the heavy-fragment multiplicity. The nuclear dissipation enhances this effect, while the survival probability of a specific mass partition is significantly increased when the source is endowed with an overall radial flow.

†Present address: Department of Physics, California Polytechnic State University, San Luis Obispo, California 93407.

*This work was supported in part by the Director, Office of Energy Research, Office of High Energy and Nuclear Physics, Division of High Energy Physics, of the U.S. Department of Energy under Contract No. DE-AC03-76SF00098.

Contents

1 Introduction **1**

2 Transition-state treatment **1**

3 Multifragment dynamics **5**
3.1 Dissipation 6
3.2 Equations of motion 7

4 Results and discussion **8**
4.1 Initial states 8
4.2 Disassembly widths 9
4.2.1 Binary fission 9
4.2.2 True multifragmentation 10
4.3 Radial flow 11
4.3.1 Fragment formation 13
4.3.2 Kinetic energy 13

5 Concluding remarks **14**

1 Introduction

In a recent paper[1], we presented a general formulation of the transformation of an excited nucleus into several interacting prefragments. Based on a generalization of the Bohr-Wheeler treatment of ordinary fission [2], that work derived expressions for the partial widths for the system to find itself in a conditional transition configuration consisting of specified heavy prefragments. Since these prefragments are not yet fully developed, the dynamical evolution of the system subsequent to the transition is expected to play a significant role: not only may the specific mass partition change as the fragments complete their formation and separate (as also occurs in ordinary binary fission), but some of them may recombine, so that the final fragment multiplicity may be smaller than that characterizing the particular transition configuration considered. It is therefore necessary to augment the transition-state formulation with a treatment of the post-transition dynamics. It is on this task this second paper is focussed.

First, the transition-state treatment developed in ref. [1] is briefly summarized in section 2. Then the specific treatment of the multifragment dynamics is described in section 3; it includes both conservative and dissipative forces and builds on experience gained from studies of damped nuclear reactions, so that no arbitrary quantities are introduced. This formal framework is then used to examine the importance of the post-transition dynamics in section 4. The treatment is also extended to accomodate the possibility of an overall radial flow (a "blast"), as might result from a compression generated early on in the nuclear collision producing the source. This aspect is relevant to the question of whether multifragmentation processes can be utilized to probe the properties of high-density matter. Finally, in section 5, we give a concluding discussion, in which we outline the most important aspects that remain to be incorporated before the theory can provide quantitative results.

2 Transition-state treatment

This section contains a summary of the transition-state treatment developed in the preceding work [1]. We consider a very excited nuclear system consisting of A nucleons and having a total energy E. After its creation, presumably by an energetic nuclear collision, this source is assumed to achieve a transient equilibrium so that statistical considerations can be employed.

Any particular manifestation of the system is described as a number of distinct but interacting prefragments. Thus, such a *fragmentation* F is characterized by the quantities $\{A_n, \mathbf{r}_n, \mathbf{p}_n, \epsilon_n, n = 1, ..., N\}$, where A_n, $\mathbf{r}_n$, $\mathbf{p}_n$, and ϵ_n denote the mass number, position, momentum, and internal excitation energy of fragment n, respectively. As in ref. [1], the isospin degree of freedom is ignored; its inclusion would be relatively straightforward, though perhaps somewhat tedious, and should not present any conceptual problems. The partial width for the idealized source to break up into a specified mass partition $A_1, ..., A_N$ is denoted by $\Gamma_{A_1 \cdots A_N}(E)$. The total width $\Gamma_A^N(E)$ for breakup into any N prefragments can then be obtained by performing a

summation over the various contributing mass partitions,

$$\Gamma_A^N(E) = \frac{1}{N!}\prod_{n=1}^{N}\left[\sum_{A_n}\right]\ \delta(\sum_{n=1}^{N} A_n - A)\ \Gamma_{A_1\cdots A_N}(E)\ , \tag{1}$$

and the total breakup width is $\Gamma_A^{\rm total}(E) = \sum_N \Gamma_A^N(E)$.

In order to make the system amenable to a transition-state treatment, we define, for a given fragmentation F, the disassembly coordinate q and its conjugate momentum p as follows,

$$q_F^2 = \frac{1}{m_0}\sum_{n=1}^{N} m_n r_n^2\ , \qquad p_F = \frac{1}{q_F}\sum_{n=1}^{N} \mathbf{p}_n\cdot\mathbf{r}_n\ , \tag{2}$$

where m_n is the fragment mass. The quantity q is simply related to the *rms* radius of the mass distribution of the total system and provides a general and convenient measure of the overall linear dimension of the multifragment system. Its conjugate momentum p is a simple measure of the outwards directed motion of the fragments (the "radial flow"). These disassembly variables can be regarded as the radial position and momentum in the $3N$-dimensional hyperspace in which the multifragment configuration can be embedded. Moreover, q and p are conjugate variables, and the associated inertial mass is given by $m_0 = \sum_n m_n$, since the kinetic energy in the disassembly degree of freedom is $k = \frac{1}{2}p\dot{q} = p^2/2m_0$.

The amount of energy available for statistical excitations is given by $E^\star = E - E^0_{1\cdots N} - V - k$, where $E^0_{1\cdots N}$ is the sum of the ground-state energies of the specified fragments and $V(\mathbf{r}_1,...,\mathbf{r}_N)$ is the potential energy associated with the particular configuration. This energy is shared between the random kinetic energy of the fragments (in addition to the energy k of their ordered outwards motion), κ, and the internal excitation, ϵ. The corresponding internal level density is denoted by $\rho_{1\cdots N}(\epsilon)$.

One may now consider the outwards probability current, *i.e.* the number of elementary multifragment states that pass by a given value of q per unit time. This quantity is given by

$$\begin{aligned}\nu_{A_1\cdots A_N}(E) &= h^3\,\frac{(2\pi m_0)^{-2}}{\Gamma(\frac{3}{2}N-2)}\prod_{n=1}^{N}\left[(\frac{m_n}{2\pi\hbar^2})^{\frac{3}{2}}\int d\mathbf{r}_n\right]\cos\alpha \\ &\times\int\frac{dp}{h}\frac{p}{m_0}\int d\epsilon\ \rho_{1\cdots N}(\epsilon)\ \kappa^{\frac{3}{2}N-3}\ \delta(\mathbf{R}_F)\ \delta(q_F-q)\ ,\end{aligned} \tag{3}$$

where $\mathbf{R}_F$ denotes the *CM* position of the fragmentation F. The flux factor p/m_0 in the p-integration can be thought of as arising from an integration over values of q extending from 0 to p/m_0, the distance covered by q per unit time. After division by Planck's constant h, the p-integral then yields the number of elementary states that pass the specified value of q per unit time. Since $(p/m_0)dp = dk$, the integrations over k and ϵ may be interchanged, so the former one can be performed analytically. The geometric factor $\cos\alpha$ corrects for the fact that in general the local normal to the transition surface may not be directed along the radius vector in the configuration hyperspace; this factor is ignored in the following (*cf.* the discussion in [1]).

It is advantageous to express the current (3) as an average over the constrained fragment positions. Invoking the formula for the surface area of a hypersphere, we find

$$\begin{aligned}
&\nu_{A_1\cdots A_N}(E) \\
&= \frac{1}{h}\frac{\sqrt{4\pi}}{\Gamma(\frac{3}{2}N-\frac{3}{2})}\,\frac{1}{\Gamma(\frac{3}{2}N-1)}\,\langle\,(\frac{m_0 q_{1\cdots N}^2}{2\hbar^2})^{\frac{3}{2}N-2}\int_0^{\epsilon_{1\cdots N}} d\epsilon\;\rho_{1\cdots N}(\epsilon)\;[\epsilon_{1\cdots N}-\epsilon]^{\frac{3}{2}N-2}\,\rangle' \\
&\approx \frac{1}{h}\,\frac{\sqrt{4\pi}}{\Gamma(\frac{3}{2}N-\frac{3}{2})}\,\langle\,(\frac{m_0 q_{1\cdots N}^2\bar{\tau}}{2\hbar^2})^{\frac{3}{2}N-2}\;\rho_{1\cdots N}(\epsilon_{1\cdots N})\;\bar{\tau}\,\rangle'\,. \qquad (4)
\end{aligned}$$

The quantity $q_{1\cdots N}$ denotes that value of q for which the current attains its minimum value, when an overall scaling of the fragment positions is performed, $\mathbf{r}_n \to \lambda\mathbf{r}_n$. At this point, the maximum internal excitation energy is $\epsilon_{1\cdots N}$, and the corresponding maximum temperature is $\tau_{1\cdots N}$. The prime indicates that the average is over fragment positions $\{\mathbf{r}_n\}$ that have been constrained to have their center-of-mass position at the origin, $\mathbf{R}_F = 0$, and have the specified *rms* extension, $q = q_{1\cdots N}$. The second relation is obtained by evaluating the ϵ-integration in the stationary-phase approximation. The corresponding most probable internal temperature $\bar{\tau}$ of the particular configuration is given by

$$\bar{\tau} = \tau_{1\cdots N}[(1+\xi^2)^{\frac{1}{2}} - \xi]\,, \qquad \xi = \frac{3N-4}{2}\,\frac{\tau_{1\cdots N}}{2\epsilon_{1\cdots N}}\,. \qquad (5)$$

For given values of the constrained positions $\{\mathbf{r}_n\}$, the integrand in the flux (3) has a minimum at some value $q_{1\cdots N}$, as a function of the scaling parameter λ. This key feature is easy to understand since the potential energy has a maximum as the system is stretched from a compact configuration towards separated fragments. This barrier top is a generalization of the conditional saddle point for asymmetric binary fission. The minimum in the integrand will be shifted slightly inwards relative to the barrier top because the geometrical factor q^{3N-4} biases the statistical weights toward larger sizes. As in the treatment of binary fission, it is natural to identify the value $q = q_{1\cdots N}$ with the local "bottle neck" in the evolution towards breakup. Accordingly, the total rate at which the system makes an irreversible transition towards disassembly is approximated by the above current (4), with the proviso that the local value of q be chosen as that for which the integrand has a minimum, *i.e.* the transition value $q_{1\cdots N}$.

Invoking the usual statistical assumption, the breakup rate of the system (into the specified mass partition) is given by the magnitude of the transition current, $\nu_{A_1\cdots A_N}(E)$, divided by the total compound level density, $\rho(A,E)$, which represents the total number of elementary states in the source. (Both of these refer to states with a total energy within an infinitesimal interval dE around the specified value E.) We then obtain the following relation for the partial width for breakup into specified prefragments,

$$\begin{aligned}
\Gamma_{A_1\cdots A_N}(E) &= h\,\frac{\nu_{A_1\cdots A_N}(E)}{\rho(A,E)} \qquad (6) \\
&\approx \frac{1}{\rho(A,E)}\,\frac{\sqrt{4\pi}}{\Gamma(\frac{3}{2}N-\frac{3}{2})}\,\langle\,(\frac{m_0 q_{1\cdots N}^2\bar{\tau}}{2\hbar^2})^{\frac{3}{2}N-2}\;\rho_{1\cdots N}(\epsilon_{1\cdots N})\;\bar{\tau}\,\rangle'\,.
\end{aligned}$$

We remind of the fact that the average should be taken over the *reduced* fragment positions describing configurations constrained to have a vanishing center-of-mass position and a specified (but arbitrary) overall *rms* extension.

The level density $\rho(A, E)$ of the source is difficult to calculate because of the many collective modes accessible at the high excitations considered. A theoretical calculation can in principle be made on the basis of the multifragment formalism developed in [3, 1], although considerable development would be required before quantitative results could be obtained. For our present purposes, we adopt a relatively simple preliminary expression, namely

$$\rho(A, E) = \chi \, \frac{4\pi}{3} r_0^3 A \, (\frac{m_0 \tau}{2\pi\hbar^2})^{\frac{3}{2}} \, \rho_A(\epsilon_0) \, , \tag{7}$$

with the value $\chi = 1$. The last quantity has the same form as the level density employed for each of the individual prefragments, which are taken to be of simple Fermi-gas type, $\rho_n(\epsilon_n) = cA_n^{-p} \exp 2\sqrt{a_n \epsilon_n}$. The factor in front is introduced as a rough attempt to take account of the fact that the prefragments in the source may roam the entire volume bounded by the appropriate transition surface. The form adopted should only be relied on for its qualitative features, and the resulting decay widths should therefore be considered as schematic only.

The formula (6) has an intuitive interpretation. It expresses the partial disassembly width Γ as the outwards transition current relative to the total number of states, as in the ordinary transition-state method. The transition current is obtained by adding the contributions from all possible reduced positions of the fragments, corresponding to an integration over the generalized orientation in hyperspace. For each such generalized orientation, the local transition flux is a product of a macroscopic and a microscopic factor. The macroscopic factor $N_{\text{macro}} \sim \sqrt{4\pi}(m_0 q^2 \tau / 2\hbar^2)^{\frac{3}{2}N-2} / \Gamma(\frac{3}{2}(N-1))$ is the effective number of states associated with the macroscopic degrees of freedom, *i.e.* those associated with the overall motion of the individual prefragments, while the second factor $N_{\text{micro}} \sim \rho\tau$ is the outwards probability current for each such macroscopic state.

At low excitation, channels with only two fragments dominate and the formula (6) for the decay width reduces to a form rather similar to the standard Bohr-Wheeler expression,[2] but with an extra factor arising from the orbital motion of the binary complex. The dominant multiplicity increases with excitation and at high excitation the treatment acquires considerable formal similarity with existing statistical multifragmentation models,[3, 4, 5] although certain notable differences are present. An important advantage of the treatment is that it automatically provides the constraint on the fragment positions so that a finite result is obtained; in this regard it is a significant advance relative to current statistical models in which the freeze-out volume must be prescribed separately. It should also be added that conservation of angular momentum can readily be incorporated into the formulation, as described in ref. [1]. Its main effect is to reduce the available energy by the amount tied up in overall rotation.

3 Multifragment dynamics

This section describes our treatment of the dynamical evolution of the disassembling multifragment system. In this endeavor, we shall exploit the considerable insight gained from many years of theoretical and experimental investigation of study of damped nuclear reactions. Indeed, the disassembling system can be regarded as a generalized damped reaction process, involving several fragments and being prepared with all the fragments near each other and with a finite temperature.

The dynamical state of the multifragment system is described by the variables

$$\{\mathbf{r}_n, \mathbf{p}_n, \mathbf{S}_n, \boldsymbol{\phi}_n, \epsilon_n, n = 1, \cdots N\} \ , \tag{8}$$

where $\mathbf{S}_n$ is the angular momentum (or spin) of a fragment and $\boldsymbol{\phi}_n$ denotes the associated conjugate set of angles specifying the spatial orientation of the fragment. Since we treat the fragments as spheres, the angles $\boldsymbol{\phi}_n$ are cyclic and hence not physically interesting. (However, we retain them in the formulation for completeness; they are in fact practically useful if one wishes to monitor the evolution by means of a graphical display (a movie), since they can be utilized as indicators of the fragment rotation.) In general the individual fragments may change their mass numbers A_n in the course of the evolution, both because of the statistical exchange nucleons (the mechanism underlying the friction employed), and as a consequence of light-particle emission (see the discussion in section 5). These effects are relatively minor for the heavy fragments of primary interest here and will be ignored for the time being.

The conservative part of the evolution of the N-fragment system is described by a Lagrangian $\mathcal{L}(\mathcal{Q}, \dot{\mathcal{Q}})$ given by

$$\mathcal{L} = \sum_{n=1}^{N} \frac{\mathbf{p}_n^2}{2m_n} + \sum_{n=1}^{N} \frac{\mathbf{S}_n^2}{2\mathcal{I}_n} - V(\mathbf{r}_1, \cdots, \mathbf{r}_N) \ , \tag{9}$$

where $\mathcal{Q}$ denotes the generalized coordinates $\{\mathbf{r}_n, \boldsymbol{\phi}_n\}$ and the dot indicates the corresponding time derivative. The dissipation generated by the motion is described by a Rayleigh function $\mathcal{F}(\mathcal{Q}, \dot{\mathcal{Q}})$. The temporal development of the system is then governed by the general Lagrange-Rayleigh equation,

$$\frac{d}{dt}\frac{\partial \mathcal{L}}{\partial \dot{\mathcal{Q}}} + \frac{\partial \mathcal{F}}{\partial \dot{\mathcal{Q}}} = \frac{\partial \mathcal{L}}{\partial \mathcal{Q}} \ . \tag{10}$$

For the conservative motion, we employ the potential energy described in ref. [1]. It is of the form

$$V(\mathbf{r}_1, \cdots, \mathbf{r}_N) = E^0_{1\ldots N} - E_0 + \sum_{n<n'}^{N} V_{nn'}(r_{nn'}) \ . \tag{11}$$

Here $E^0_{1\ldots N} = \sum_n E^0_n$ is the sum of the ground-state energies of the N fragment products, and E_0 is the ground-state energy of the disassembling compound system. Moreover, $V_{nn'}$ is the interaction potential between the two fragments n and n'. This latter quantity has been carefully designed so as to yield a reasonable reproduction

of the shapes and energies of the conditional binary saddles throughout the nuclear chart, by employing a simple parametrization developed by Swiatecki.[6]

Finally, the inertial mass of a given fragment is approximated by $m_n = A_n m_N$, where m_N is the nucleon mass, and the moment of inertia is taken as $\mathcal{I}_n = \frac{2}{5} m_n R_n^2$, corresponding to a sharp rigid sphere.

3.1 Dissipation

Extensive investigations of damped nuclear reactions have shown that the interfragment forces are dissipative. Our treatment of the nuclear dissipation is based on the the nucleon-exchange transport model in which the dissipation is generated by the stochastic exchange of nucleons between the interacting nucleides.[7] This model has been found to give a good overall reproduction of a large variety of damped reaction observables.[8] Thus, the friction forces are derived from a Rayleigh function of the form

$$\mathcal{F} = \frac{1}{2} \sum_{n<n'}^{N} \dot{Q}_{nn'} = n_0 \sum_{n<n'}^{N} \sigma_{nn'}(r_{nn'})[2(u_{nn'}^{\rm rad})^2 + (u_{nn'}^{\rm tan})^2] \ . \tag{12}$$

Here $\dot{Q}_{nn'}$ is the dissipation arising from the exchange of nucleons between the fragments n and n'. In the following this quantity will be described in some detail; for notational convenience we denote the two nuclei considered by A and B, as is commonly done in the context of damped nuclear reactions.

In the friction form factor, the quantity $n_0 = \frac{1}{4}\rho\bar{v} \approx 0.263/\mathrm{fm}^2/10^{-22}$ s is the one-sided nucleon flux in standard nuclear matter and σ_{AB} is the effective window area through which the nucleons are exchanged between the two nuclei. In the present treatment, we adopt the following simple form,

$$\sigma_{AB} = 2\pi \bar{R} b \Psi(\frac{s}{b}) \ , \tag{13}$$

suggested by the proximity approximation.[9] Here $b \approx 1$ fm is the nuclear surface diffuseness, and the reduced radius $\bar{R}$ is given in terms of the radii R_A and R_B of the individual nuclei as $\bar{R} = R_A R_B/(R_A + R_B)$, ignoring the difference between the central radius C and the equivalent sharp radius R. The smallest separation between the two nuclear surfaces is then given by $s = R - R_A - R_B$. Finally, the dimensionless form factor $\Psi(\zeta)$ is taken to have the form

$$\Psi(\zeta) = \begin{cases} \zeta \leq 0: & 1.4 - \zeta \\ \zeta \geq 0: & 1.4 \ \exp(-\zeta) \end{cases} \ . \tag{14}$$

This form is adopted for simplicity and corresponds approximately to what would be expected for two spherical fragments with a small surface separation. The possible existence of a neck between the two fragments is not taken into account, although this may be a required for quantitative applications.

In the expression (12) for the dissipation rate, the quantities $u_{ab}^{\rm rad}$ and $u_{ab}^{\rm tan}$ denote the radial and tangential components of the relative surface velocity, in the interaction

zone where the nucleons are exchanged. Since the fragments are considered to be rigid, the relative radial velocity is given by

$$\mathbf{U}_{ab}^{\mathrm{rad}} = \mathbf{U}_{AB} \cdot \hat{\mathbf{r}}_{AB}\, \hat{\mathbf{r}}_{AB} \ , \tag{15}$$

where $\mathbf{r}_{AB} = \mathbf{r}_A - \mathbf{r}_B$ is the relative position of the two fragments and $\mathbf{U}_{AB} = \dot{\mathbf{r}}_{AB}$ is the relative fragment velocity. (The hat indicates a unit vector, $\hat{\mathbf{r}} = \mathbf{r}/r$.) The tangential component of the relative center velocity is then given by $\mathbf{U}_{AB}^{\mathrm{tan}} = \mathbf{U}_{AB} - \mathbf{U}_{AB}^{\mathrm{rad}}$. If the fragments do not rotate this quantity represents the tangential part of the relative velocity of the two fragment surfaces. However, since the fragments carry angular momenta, $\mathbf{S}_A$ and $\mathbf{S}_B$, they are rotating and this feature modifies the relative surface velocity. Therefore, in general

$$\mathbf{u}_{ab}^{\mathrm{tan}} = \mathbf{U}_{AB}^{\mathrm{tan}} + \mathbf{u}_a - \mathbf{u}_b \ , \tag{16}$$

where $\mathbf{u}_a = \boldsymbol{\omega}_A \times \boldsymbol{\rho}_a$ is the velocity of the surface of fragment A, and $\mathbf{u}_b = \boldsymbol{\omega}_B \times \boldsymbol{\rho}_b$ is the velocity of the surface of fragment B, both as seen from the respective fragment center. Here $\boldsymbol{\omega}_A = \mathbf{S}_A/\mathcal{I}_A = \dot{\boldsymbol{\phi}}_A$ and $\boldsymbol{\omega}_B = \mathbf{S}_B/\mathcal{I}_B = \dot{\boldsymbol{\phi}}_B$ are the angular velocities of the two fragments. Furthermore, the location of the interaction zone between the two fragments is

$$\boldsymbol{\rho}_{BA} = -\frac{R_A}{R_A + R_B}\, \mathbf{r}_{AB} \ , \qquad \boldsymbol{\rho}_{AB} = \frac{R_B}{R_A + R_B}\, \mathbf{r}_{AB} \ , \tag{17}$$

as seen from the centers of the two fragments A and B, respectively.

3.2 Equations of motion

By introducing generalized momenta $\mathcal{P} \equiv \partial\mathcal{L}/\partial\dot{\mathcal{Q}}$, the above second-order Lagrange-Rayleigh equation (10) can be reduced to a set of coupled first-order equations which are computationally more convenient. Thus we get

$$\dot{\mathbf{r}}_n = \mathbf{U}_n = \frac{\mathbf{p}_n}{m_n} \ , \tag{18}$$

$$\dot{\boldsymbol{\phi}}_n = \boldsymbol{\omega}_n = \frac{\mathbf{S}_n}{\mathcal{I}_n} \ , \tag{19}$$

for the evolution of the coordinates, and

$$\dot{\mathbf{p}}_n = -\sum_{n'}{}' [\frac{\partial V_{nn'}}{\partial r_{nn'}} \hat{\mathbf{r}}_{nn'} + n_0 \sigma_{nn'} (2\mathbf{u}_{nn'}^{\mathrm{rad}} + \mathbf{u}_{nn'}^{\mathrm{tan}})] \ , \tag{20}$$

$$\dot{\mathbf{S}}_n = n_0 \sum_{n'}{}' \sigma_{nn'} \mathbf{u}_{nn'} \times \boldsymbol{\rho}_{n'n} \ , \tag{21}$$

for the evolution of the corresponding generalized momenta.

Because of the dissipation, the energy in the above degrees of freedom is not conserved but decreases steadily in the course of the evolution. This energy is dissipated from the macroscopic degrees of freedom into internal excitation of the residual microscopic degrees of freeedom. It is assumed that this energy is shared equally between

the two fragments producing it. The excitation energy of the individual fragments then evolve according to the equation

$$\dot{\epsilon}_n = \frac{1}{2}\sum_{n'}{}' \dot{Q}_{nn'} = \frac{1}{2} n_0 \sum_{n'} \sigma_{nn'} [2(u_{nn'}^{\mathrm{rad}})^2 + (u_{nn'}^{\mathrm{tan}})^2] \ . \tag{22}$$

The total rate of energy dissipation is given by $\dot{Q} = 2\mathcal{F} = \sum_n \dot{\epsilon}_n$.

It should be noted that the presence of a dissipative agency, in the present model the stochastic exchange of nucleons, gives the dynamical evolution a diffusive character. In the present investigation, we consider only the mean trajectory, which is governed by the above deterministic equations. The associated development of fluctuations and correlations can be incorporated by adapting the transport treatment developed for damped reactions.[7] Generally, the accumulated fluctuations in the fragment masses are relatively small and so have little bearing on our present study.

4 Results and discussion

The above closed set of equations can be readily solved to yield the dynamical evolution of the system, starting from any specified multifragment transition state, F.

4.1 Initial states

For specified prefragment mass numbers, $A_1, ..., A_N$, a sample of transition-state configurations is chosen randomly in accordance with the expression (6). This amounts to first selecting the N prefragment positions $\mathbf{r}_n$ randomly, subject to the constraints that the overall center of mass $\mathbf{R}_F$ be at the origin and the overall *rms* size q_F be equal to an arbitrary but fixed value q_0, and then performing a scale transformation $\mathbf{r}_n \rightarrow (q_{1...N}/q_0)\mathbf{r}_n$ to bring the configuration to the transition surface (where the current $\nu_{1...N}$ has a minimum).

In our formulation of the transition-state treatment [1], the transition configurations are determined as those for which the overall outwards flux has a minimum. This simple assumption was made mainly to facilitate the formal developments which have a general applicability. As we now combine such statistical considerations with the dynamical features of the disassembling nuclear system, we need to modify the formulation appropriately. The basic assumption underlying the transition-state method is that the disassembling system maintains global statistical equilibrium among all configurations inside the transition surface. Physically, such a situation can only be reasonably expected to prevail if the system is well connected, that is to say, if the prefragments are situated within the proximity of one another. An inspection of samples of candidate transition configurations reveals, not surprisingly, that the assumption of global equilibrium often appears to be invalidated. Most typically, one fragment is positioned away from the rest, at such a distance that little exchange of energy and momentum can occur.

In order to address this problem in a quantitative and systematic manner, we perform a cluster analysis of the multifragment configuration. Towards this end, we

consider two fragments to be *linked* iff their surface separation is smaller than a certain value, $s_0 = 2$ fm, representing the maximum distance for which the the fragments can be expected to maintain mutual equilibrium (by the exchange of nucleons through the "window" between them).

On the basis of this definition, any multifragment configuration can be considered as a mathematical *graph*, which can be subjected to decomposition into isolated clusters. Such a *cluster* then consists of fragments that are all in communication with each other via a succession of binary links as defined above. On the basis of this cluster analysis, we may now reject candidate transition configurations that consist of two or more isolated clusters, since no equilibrium can be maintained between the disconnected clusters. In other words, from the general class of candidate transition configurations defined as in [1] by means of the outwards flux, we accept only those that form a single connected cluster. Our further discussion is based on results obtained with this restriction.

Having thus found an acceptable transition configuration, the initial dynamical state is prepared by endowing the prefragments with linear and angular momenta. The linear momenta $\mathbf{p}_n$ have an approximately canonical distribution characterized by the most probable local temperature $\bar{\tau}$ given in (5), although only those states that have a positive value of the overall outwards momentum p_F should be accepted. Having selected the momenta, a modified local temperature is calculated and the fragment spins $\mathbf{S}_n$ are selected from the corresponding canonical distribution, which is a very good approximation. Finally, the remaining excitation energy ϵ is distributed on the N fragments in proportion to their heat capacity, $\epsilon_n \sim a_n$, so that they all have the same temperature τ_n at the outset.

4.2 Disassembly widths

We are now in a position to study the effect of the post-transition dynamics. Figure 1 shows the calculated transition width $\Gamma_{A_1 \cdots A_N}(E)$ for a number of specified mass partitions of a system with $A = 120$, shown as a function of the excitation energy per nucleon in the source, $E^\star/A$. These results have been calculated without considering the dissipative forces, in order to provide a simple reference. Figure 2 then shows the effect of including the proximity friction induced by nucleon exchange.

4.2.1 Binary fission

Let us first discuss the binary transition channels, *i.e.* those disassembly processes for which the transition configuration consists of two prefragments, corresponding to ordinary fission. We observe that as $E^\star/A$ is increased from one to ten MeV, the corresponding fission widths $\Gamma_{A_1 A_2}$ grow by about four orders of magnitude, approaching about a few hundred electron Volts, and the widths for the different mass partitions are within half an order of magnitude of each other. (We wish to recall that the absolute magnitude is rather uncertain because of our rudimentary knowledge of the source level density entering in the denominator of the Bohr-Wheeler formula.) Because of the relatively moderate dependence of Γ on mass partition, we shall limit

our considerations to a few "typical" channels in the following discussion.

For the binary channels the effect of the dissipation is relatively unimportant: once the two prefragments have receded beyond their respective barrier separation, they must keep moving apart. The dissipative effect in then limited to the conversion of relative kinetic energy into internal excitation. In reality there is also a certain amount of mass diffusion during the descent from saddle to scission, but this process is not considered in the present study, since it is relatively unimportant. (From studies of induced fission and damped reactions we know that the degree of mass diffusion is relatively small, so that the character of the particular channel will change little; in particular, the (pre)fragment multiplicity would be unaffected, *cf.* the remarks at the end of section 3.)

It should be noted, though, that since the transition point lies (slightly) inside the saddle point (because of the additional macroscopic factor $\sim q^2$ in our expression for Γ), the friction may actually prevent the system from surmounting the barrier top, when the radial kinetic energy is sufficiently low. The two prefragments will then recombine and the given transition configuration does in fact not lead to disassembly. Because of this effect, the actual fission widths are smaller than the corresponding transition widths. For binary channels this effect is very small, as is evident from fig. 2, and can usually be ignored, but for higher multiplicities it grows increasingly significant, as we shall demonstrate, and must be taken into account.

4.2.2 True multifragmentation

Let us now turn to true multifragmentation, *i.e.* processes involving more than two fragments. The most important effect of the dynamics is that some of the prefragments may fuse. Those processes for which such recombination occurs lead to final states having a correspondingly lower fragment multiplicity and thus, in principle, they contribute to the disassembly widths for those channels. The width for the source to disassemble into the a specified mass partition $A_1 \cdots A_N$ can then be written on the form

$$\begin{aligned} \Gamma^{\text{dissassembly}}_{A_1\cdots A_N}(E) &= \Gamma^{\text{transition}}_{A_1\cdots A_N}(E)\; P(\alpha \to \alpha) \\ &+ \sum_{N'>N} \frac{1}{N'!} \prod_{n=1}^{N'} \left[\sum_{A'_n}\right] \delta(\sum_{n=1}^{N'} A'_n - A)\; \Gamma^{\text{transition}}_{A'_1\cdots A'_{N'}}(E)\; P(\alpha' \to \alpha) \end{aligned} \tag{23}$$

Here the $\Gamma^{\text{transition}}_{A'_1\cdots A'_{N'}}(E)$ denotes the partial width for the source to transform itself into a specified mass partition $\alpha' = A'_1 \cdots A'_{N'}$ at the transition point; this is the quantity given in eq. (6). The probability that this initial mass partition evolves into the specified final mass partition $\alpha = A_1 \cdots A_N$ is given by $P(\alpha' \to \alpha)$. The total width $\Gamma^{\text{dissassembly}}_{A_1\cdots A_N}(E)$ for disassembly into a particular mass partition, irrespectively of the initial specification, can then be obtained by adding up the partial widths for all possible precurser partitions α', each weighted with the associated transmission probability $P(\alpha' \to \alpha)$. In the above expression, the first term is the direct contribution $\alpha \to \alpha$ arising from the survival of the desired mass partition α, while the

second line contains the indirect feeding $\alpha' \rightarrow \alpha$ from transition states α' with a larger multiplicity for which some prefragments fuse.

In the present discussion, we shall disregard the indirect terms in (23). Contributions from side feeding are not necessarily negligible, though, but their proper inclusion would require the development of a more accurate description of the recombination processes. (In our present calculations, two fusing prefragments are treated as two distinct entities throughout and so the interaction of the complex with a third prefragment is not very accurate.)

Figure 1 shows the disassembly widths calculated for two ternary and two quaternary mass partitions. For a given multiplicity, Γ is not very sensitive to the particular mass partition, which simplifies the analysis. The ternary widths rise more steeply than the binary widths, and the quaternary widths are still steeper, as is generally expected because of the macroscopic factor $N_{\text{macro}} \sim q^{3N-4}$ in the transition current. They catch up with the binary widths at around $E^{\star}/A = 9$ MeV. It should be recalled that the total disassembly width Γ_N for obtaining a given multiplicity N is obtained by adding the contributions from all possible partitions of the source into N fragments, see eq. (1). Since the number of mass partitions increases rapidly with multiplicity, the values for the total widths Γ_N will be correspondingly larger.

As mentioned above, for higher multiplicities there exists the possibility that some prefragments may fuse in the course of the disassembly process, thus reducing the heavy-fragment multiplicity. Generally, the dissipation acts to facilitate fusion and the corresponding reduction of the width $\Gamma_{A_1 \cdots A_N}$ is significant.

This is illustrated in fig. 2 for the mass partitions 20+40+60 and 15+25+35+45. For ternary channels the associated reduction is about one order of magnitude, while it is about one and a half order of magnitude for quaternary channels. The effect grows progressively larger for higher multiplicities. In fact, for the higher multiplicities, the probability that the initial multiplicity survives the post-transition dynamics becomes negligible, and the major portion of the yield for a given mass partition arises indirectly by "side feeding" from transition configurations that had initially more prefragments but suffered a reduction in multiplicity due to fusion. Because of this general feature, there is no simple relationship between the transition configuration and the final multifragment state and the post-transition dynamics plays an indispensable role in the disassembly process.

Of course, one might still attempt to describe phenomenologically the outcome of this complicated dynamical disassembly process in terms of a simple freeze-out model, by fitting its parameters appropriately. While such an undertaking may provide a useful means for systematizing the data, our present studies indicate that the insight gained about the disassembling system would be somewhat limited.

4.3 Radial flow

A major focal point in the study of intermediate-energy nuclear collisions is the exploration of the nuclear equation of state. Particular efforts have been directed towards extracting the compressibility of nuclear matter. It is generally expected that the early stage of energetic nuclear collision leads to significant enhancements of the den-

sity, relative to the standard saturation value of ≈ 0.17 fm^{-3}. Such a compression may in turn produce an overall radial flow in the system at the subsequent disassembly stage. Our multifragmentation treatment can readily be employed to study the effect of such a feature, if it were indeed present.

For this purpose, it is convenient to characterize the degree of overall outwards motion by the "blast" energy $E_{\rm blast} = p_0^2/2m$, where p_0 is the amount of superimposed radial momentum. The ordinary transition-state treatment described above corresponds to $E_{\rm blast} = 0$. For a specified finite value of $E_{\rm blast}$, we employ the following modified procedure.

The transition configuration (*i.e.* the prefragment positions $\mathbf{r}_n$) is determined in the standard manner, but the prefragment momenta $\mathbf{p}_n$ are picked differently. First, the available energy at the transition point is reduced by the specified blast energy, $\epsilon'_{1\ldots N} = \epsilon_{1\ldots N} - E_{\rm blast}$, and the associated temperature $\bar{\tau}'$ is corresponding smaller. A set of "local" fragment momenta $\{\mathbf{p}'_n\}$ are then sampled from a distribution characterized by the reduced temperature $\bar{\tau}'$. These local momenta are isotropic and correspond to what would be seen in a frame moving outwards with the specified blast velocity, which is equal to $(p_0/m_0)(\mathbf{r}_n/q_0)$ locally. The actual prefragment momenta $\mathbf{p}_n$ are finally obtained by superimposing the blast motion,

$$\mathbf{p}_n = \frac{m_n p_0}{m_0 q_0}\,\mathbf{r}_n + \mathbf{p}'_n\ , \tag{24}$$

with usual the proviso that only positive values of the resulting radial flow be admitted, $p > 0$ (otherwise new local momenta $\mathbf{p}'_n$ are picked and the procedure is repeated). As the value of the blast energy $E_{\rm blast}$ is increased, a larger proportion of the energy is tied up in the collective flow and the random components of the fragment momenta become corresponding smaller. Therefore, for large values of $E_{\rm blast}$ the random components $\mathbf{p}'_n$ of the admitted states are relatively small (and practically isotropic), while the total momenta $\mathbf{p}_n$ are nearly perfectly radially directed.

With a radial blast incorporated as described above, we now reconsider the disassembly of the $A = 120$ source. Because of the ordered outwards motion, the prefragments are less likely to recombine during the dynamical evolution. Figure 3 shows the partial widths $\Gamma_{A_1\ldots A_N}$ obtained for various blast scenarios, for the specific mass partitions $40 + 80$, $20 + 40 + 60$ and $15 + 25 + 35 + 45$.

It is seen that the presence of an overall radial flow at the transition point significantly increases the survival probability of a particular configuration and, consequently, it will act to increase the corresponding partial width. It should also be noted that such a blast-induced increase in the multifragmentation width is accompanied by a decrease of sequential decays because of the associated reduction of the internal excitation energy.

It is apparent from fig. 3 that a relatively small amount of radial flow, a fraction of an MeV per nucleon, sufficies to cause a significant increase in Γ. Moreover, the effect rapidly saturates as a function of $E_{\rm blast}$. Interestingly, the values thus achieved are relatively similar to those first calculated without considering dissipation, see fig. 1. Thus dissipation and radial flow approximately counterbalance each other, with regard to the partial disassembly width $\Gamma_{A_1\ldots A_N}$.

4.3.1 Fragment formation

The fact that we have an explicit dynamical description enables us to elucidate various aspects of the disassembly dynamics. In particular, we may examine the time evolution of the fragmentation: the gradual evolution of a single well-connected cluster of prefragments to a number of individual fragments.

For this purpose it is instructive to perform a cluster analysis of the developing multifragment system. Towards this end, we regard two fragments as being *linked* iff their center separation is smaller than the value associated with their respective barrier top. In analogy to the cluster analysis made in connection with the preparation of the initial states, the dynamical fragment configurations can now be decomposed into isolated irreducible clusters. In particular, the specified mass partition $A_1 \cdots A_N$ can be regarded as fully formed when there are no longer any links present, *i.e.* when the multiplicity of irreducible clusters is equal to the number of specified prefragments.

Weighting each dynamical history in accordance with the expression (6) for the transition width, it is possible to calculate the average cluster multiplicity $< N >$, as a function of the time elapsed since the transition to the specified initial configuration occurred. Figure 4 shows the evolution of $< N >$ for the particular breakup $120 \rightarrow 16 + 20 + 24 + 28 + 32$ at $E^\star/A = 8$ MeV. It is seen that the inclusion of dissipation has little effect on $< N >$. This brings out the fact that by far the largest proportion of the initial sample evolves into final states of lower multiplicity and it is rather unlikely that a given state will emerge with its multiplicity intact. For these atypical latter states the dissipation plays a major role, as already discussed.

The figure also shows that the presence of radial flow leads to a higher multiplicity, as would be expected. Again, there is little dependence on the amount of radial flow, as soon as $E_{\text{blast}}/A > 0.5$ MeV.

4.3.2 Kinetic energy

It is also instructive to consider the time dependence of the total kinetic energy associated with the translational motion of the fragments, $E_{\text{kin}} = \sum_n p_n^2/2m_n$. The average of this quantity can be calculated using (6) as for $< N >$ above. It is displayed in fig. 5 as a function of the time elapsed since the system was started off, for the particular partition $120 \rightarrow 20+40+60$ and for various degrees of source excitation $E^\star$ and radial flow E_{blast}. Remarkably, the kinetic energy is relatively independent of the total excitation but depends predominantly on the flow. A number of details should be noted, though. First, the initial decrease in $< E_{\text{kin}} >$ is caused by the concerted action of conservative and dissipative forces as the system is moving over the barrier top. The subsequent increase is a reflection of the Coulomb-induced acceleration as the fragments recede. In the absence of flow, there is a modest increase in $< E_{\text{kin}} >$ with excitation, due to the thermal increase in the initial value of the radial momentum p. When a radial flow is present, an increase in excitation acts to increase the random component in the initial momenta and thus degrade the outwards motion. Therefore the kinetic energy is reduced as $E^\star$ grows.

The results shown in fig. 5 indicate that the initial collective flow is not degraded significantly in the course of the post-transition dynamics. The feature is further

illustrated in fig. 6, where $< E_{\rm kin} >$ is plotted as a function of the assumed amount of radial flow, for a variety of multiplicities and excitations. It is noteworthy that a fairly universal curve emerges, within a certain tolerance that is relatively largest for small flow values. This striking feature may prove useful in the analysis of experimental data on multifragmentation processes, since, taken at face value, the displayed relationship would enable the experimentalist to deduce the approximate amount of radial flow energy from the "observed" total kinetic energy. (Of course, $< E_{\rm kin} >$ is not directly observed, because of the subsequent decay processes, but it can in principle be deduced by reconstruction, provided a sufficiently exclusive measurement is made.) If the initial compression indeed produces a radial blast, it may thus be possible to probe the degree of compression achieved by examining the velocity distribution of the emerging fragments. It should be recalled, though, that our present exploratory calculations have been made with the simple proximity friction (13) which ignores the possibility of a neck between two fragments. The inclusion of a neck may significantly increase the dissipation, thus reducing the signal, and it therefore deserves consideration before a definite statement can be made.

5 Concluding remarks

In this paper and the preceding one [1], we have developed the basic elements of a statistical theory for nuclear multifragmentation. A statistical model provides a relatively well-defined reference that can be useful even if the idealized conditions are not realized in the actual processes accessible for study. The present theory combines a generalized transition-state treatment of the transformation of a source into interacting prefragments with a dynamical description of their further fate. There are a number of aspects that need further consideration, before the theory can provide quantitatively useful results. These are briefly outlined below.

The quantitative reliability of the calculations depend on the accuracy of the potential energy functional $V_{1\ldots N}$ and the internal level density $\rho_{1\ldots N}(\epsilon)$. So far, we have employed rather schematic expressions for these quantities, in order to make it possible to move forward with the formal developments. Just as the Bohr-Wheeler treatment *per se* is independent of the degree of refinement invoked when calculating the barrier heights and the level densities, so does our treatment not depend on these specific ingredients, although any numerical results of course are affected. There is still considerable work ahead towards developing a suitable potential energy functional for multifragmenting systems and their associated internal level densities. To put this task in perspective, it is may be noted that even fifty years after the advent of the Bohr-Wheeler treatment, our ability to calculate fission barriers and internal level densities is still not entirely satisfactory.

A vapor of nucleons interspersed between the prefragments should be incorporated in the description. This is particularly important, and difficult, at the higher temperatures where evaporation is significant on a time scale comparable to the global disassembly time. This problem is of general interest in the context of the nuclear equation of state at subsaturation densities and is currently being investigated.

The prefragments, which are assumed to be fairly heavy (having $A_n > 10$, say), are typically so highly excited that not only nucleons but also light composite fragments are likely to be emitted during the dynamical disassembly. Such processes can relatively easily be incorporated by augmenting the dynamical equations for the prefragments with equations describing the radiation of light fragments of specified type, such as neutrons, protons, and α-particles. In addition to yielding information about the early contribution to the light-particle yields (associated with the high-energy end of the spectra), the light-particle radiation acts back on the explicitly treated heavy fragments by continually reducing their mass and temperature. At the relatively high temperatures where multifragmentation is important, these effects may well be significant.

When light-particle emission grows copious, it may be necessary to consider the possibility of reabsorption of any emitted light fragments. This is probably most easily done by direct simulation; the trajectories of individual light ejectiles can then readily be followed and their ultimate fate established. Such an extension of the dynamics is not expected to reduce the computational speed appreciably.

Of course, the further fate of the fragments, after their decoupling from of the system, needs to be considered in a treatment aimed at direct contact with measurable fragment observables. The post-transition dynamics generally causes some fragments combine into clusters which, if they survive the early disassembly process, are likely to fuse into a secondary source. When sufficiently excited, such secondary sources should be subjected to the same disassembly treatment as the original source, and this iterative procedure should be repeated until more conventional decay processes, such as light-particle emission and ordinary fission, become dominant.

It should emphasized that the present treatment is only expected to be accurate in situations where the life time of the source is sufficiently long to permit a considerable degree of equilibration to occur, and yet shorter than the life times of the produced fragments. These idealized circumstances may not exist in systems produced in energetic nuclear collisions and the theory should be regarded as merely a useful (and relatively well-defined) reference. Our present studies have clearly demonstrated that the incorporation of dynamics is necessary, even in a statistical approach. It may be instructive to compare the present statistical and macroscopic model with a fully dynamical and microscopic model, such as the one in ref. [10] which evolves an ensemble of one-body distributions within the time-dependent Hartree-Fock approximation.

As the detector technology advances and powerful multifragment detector systems are being constructed, there are growing demands on theory to provide the tools necessary for making informative analysis of the data. The present theory, though yet incomplete, may prove useful for attempts to investigate the extent to which interesting properties of a produced source, such as a collective flow, are manifested in quantities amenable to experimental measurement.

This work was supported by the Director, Office of Energy Research, Office of High Energy and Nuclear Physics, Division of High Energy Physics, of the U.S. Department of Energy under Contract No. DE-AC03-76SF00098.

References

[1] López and Randrup, Nucl. Phys. **A000** (1989) xxx (in press)

[2] N. Bohr and J.A. Wheeler, Phys. Rev. **56** (1939) 426

[3] S.E. Koonin and J. Randrup, Nucl. Phys. **A474** (1987) 173; **A471** (1987) 355c

[4] D.H.E. Gross, Phys. Lett. **161B** (1985) 47; D.H.E. Gross, Zhang Xiao-ze, and Xu Shu-yan, Phys. Rev. Lett. **56** (1986) 1544

[5] J.P. Bondorf, R. Donangelo, I.N. Mishustin, C.J. Pethick, and H. Schulz, Nucl. Phys. **A443** (1985) 321; J.P. Bondorf, R. Donangelo, I.N. Mishustin, and H. Schulz, Nucl. Phys. **A444** (1985) 460

[6] W.J. Świątecki, Phys. Scrip. **24** (1981) 113 and private communication (1988)

[7] J. Randrup, Nucl. Phys. **A327** (1979) 490

[8] See, for example, Wolfgang U. Schröder and John R. Huizenga, *Treatise on Heavy Ion Science*, Vol. **2** (Plenum, New York, 1984)

[9] J. Randrup, Ann. Phys. **112** (1978) 356

[10] J. Knoll and J.S. Wu, Nucl. Phys. **A481** (1988) 173

Figure 1: Disassembly widths

The logarithm of the partial width $\Gamma_{A_1 \cdots A_N}$ for disassembly of a source with $A = 120$ into specified mass partitions as indicated. The abscissa is the excitation energy of the source, $E^\star$, divided by its nucleon number A. The nuclear dissipation has been ignored, and no side feeding has been considered.

Figure 2: Effect of dissipation

The logarithm of the partial width $\Gamma_{A_1 \cdots A_N}$ for disassembly of a source with $A = 120$ into the mass partitions $40 + 80$, $20 + 40 + 60$, and $15 + 25 + 35 + 45$. For a given mass partition, the upper curve is calculated without dissipation, as in fig. 1, while the lower curve results when the proximity friction (12) is included.

Figure 3: Effect of radial flow

For the mass partitions indicated, the logarithm of the disassembly width is calculated for various amounts of radial flow, as specified by the blast energy E_{blast}. For $N = 2$ the (small) effect is shown in a limited domain only, and for $N = 4$ the results obtained with $E_{\text{blast}}/A = 0.5, 2$ MeV are shown only at $E^\star/A = 5$ MeV, to avoid cluttering the display.

Figure 4: Fragment formation

The mean value of the cluster multiplicity is shown as a function of the time elapsed since a source with $A = 120$ and $E^\star/A = 8$ MeV broke up into the partition $16 + 20 + 24 + 28 + 32$, for a variety of dynamical scenarios. For a given multifragment configuration, the number of clusters is determined by performing a cluster analysis of the graph defined by the separation-dependent links between pairs of prefragments, as described in section 4.3.1. The statistical error on $< N >$ is around 0.2.

Figure 5: Evolution of kinetic energies

The average total kinetic energy $< E_{\text{kin}} >$ carried by the prefragments is shown as a function of the time elapsed since the system was at the transition point with the mass partition $20 + 40 + 60$. Results for a variety of source excitations $E^\star$ and blast energies E_{blast} are shown.

Figure 6: Kinetic energies

The average total kinetic energy of the fragments in the disassembling system, for various combinations of mass partition and excitation, as a function of the specified flow energy E_{blast}. The values of E_{kin} have been extracted at the time $t = 20 \cdot 10^{-22}$ s; at this time the fragments are well separated but their further recession under the influence of their mutual Coulomb repulsion will add several MeV to $< E_{\text{kin}} >$. The statistical error on $< E_{\text{kin}} >$ is less than the width of the band of curves.

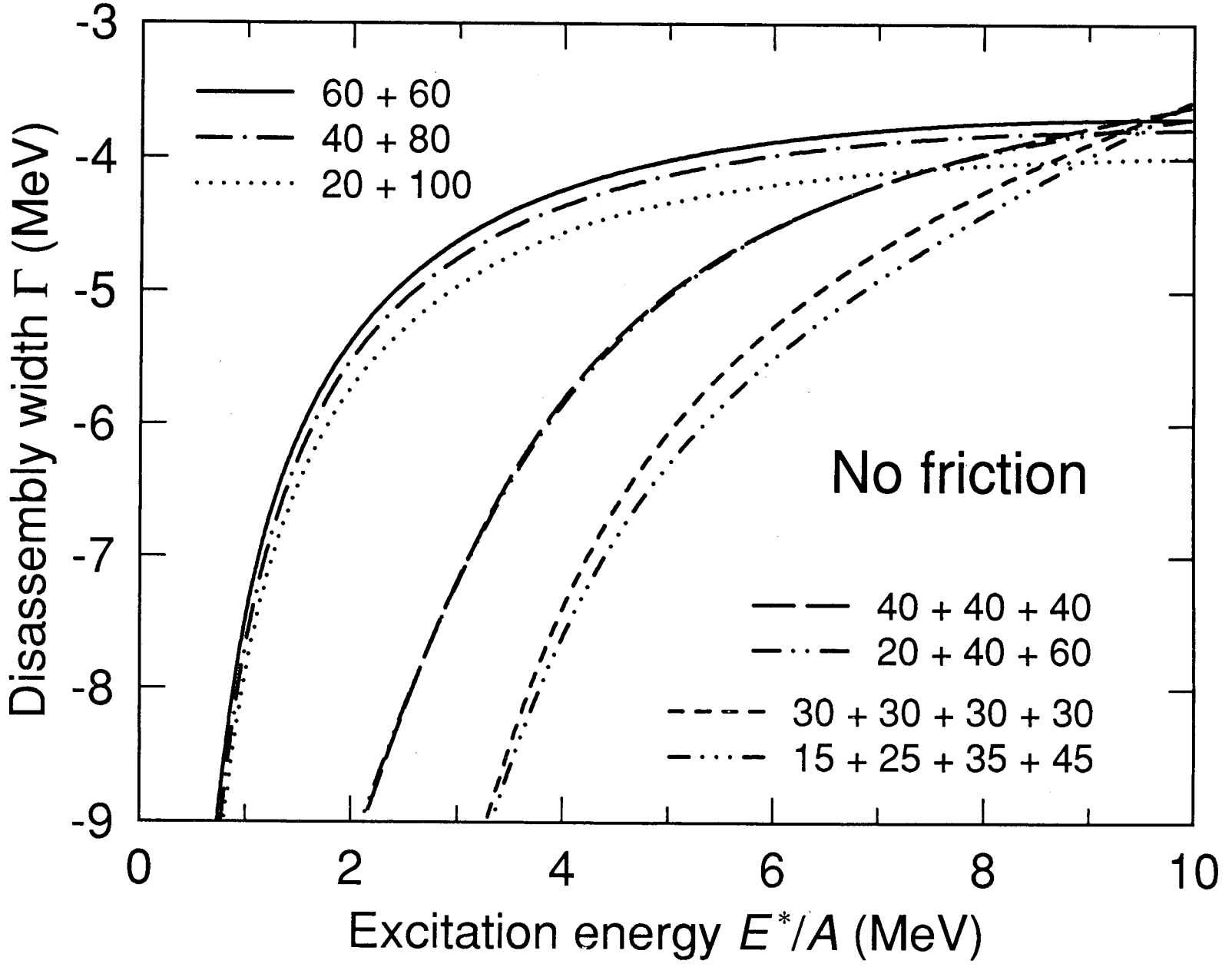
-3
-4
-5
-6
-7
-8
-9
0
2
4
6
8
10
Disassembly width Γ (MeV)
Excitation energy E*/A (MeV)
60 + 60
40 + 80
20 + 100
No friction
40 + 40 + 40
20 + 40 + 60
30 + 30 + 30 + 30
15 + 25 + 35 + 45

Figure 1

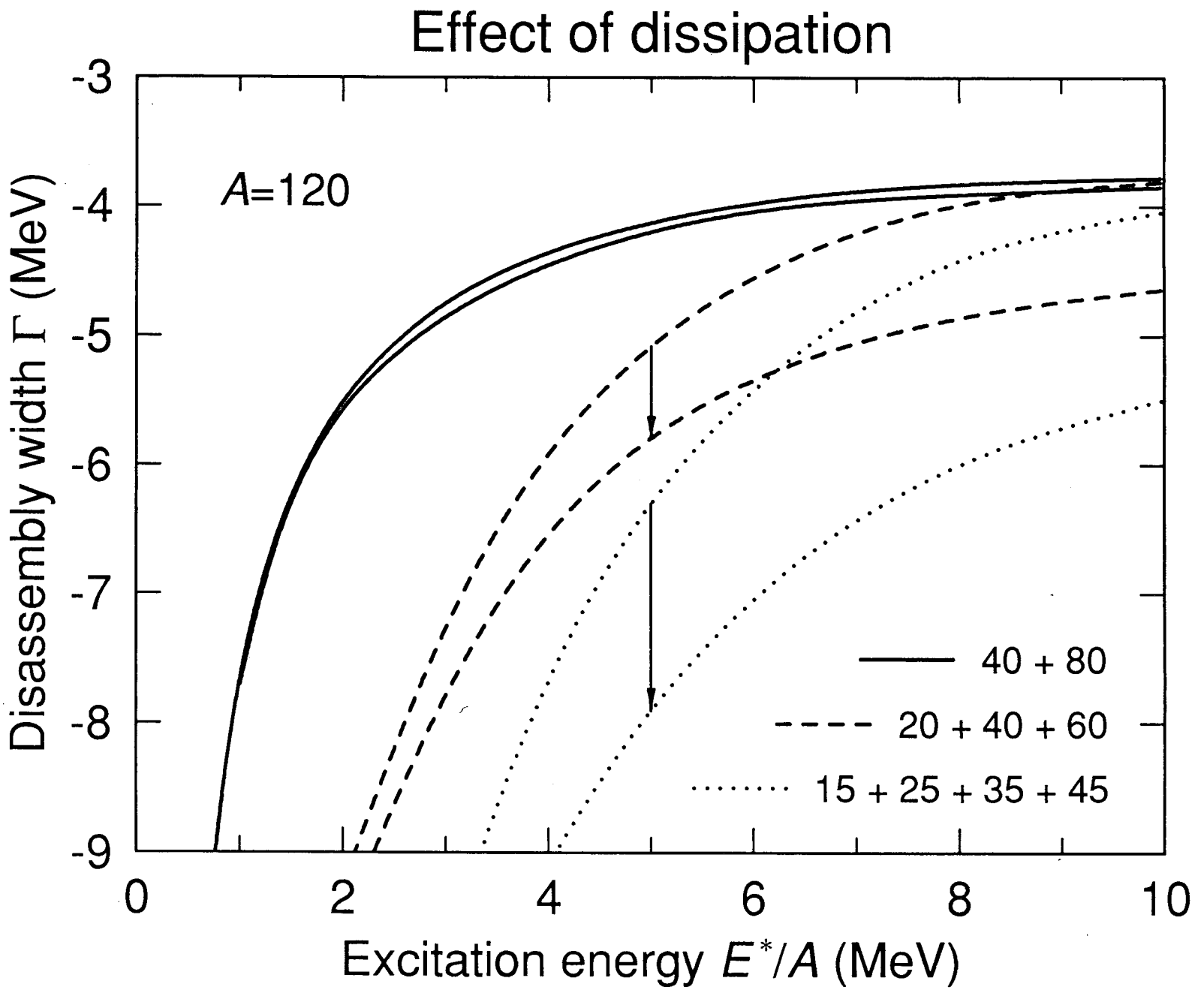
Effect of dissipation
A=120
Disassembly width Γ (MeV)
-3
-4
-5
-6
-7
-8
-9
0
2
4
6
8
10
Excitation energy E*/A (MeV)
40 + 80
20 + 40 + 60
15 + 25 + 35 + 45

Figure 2

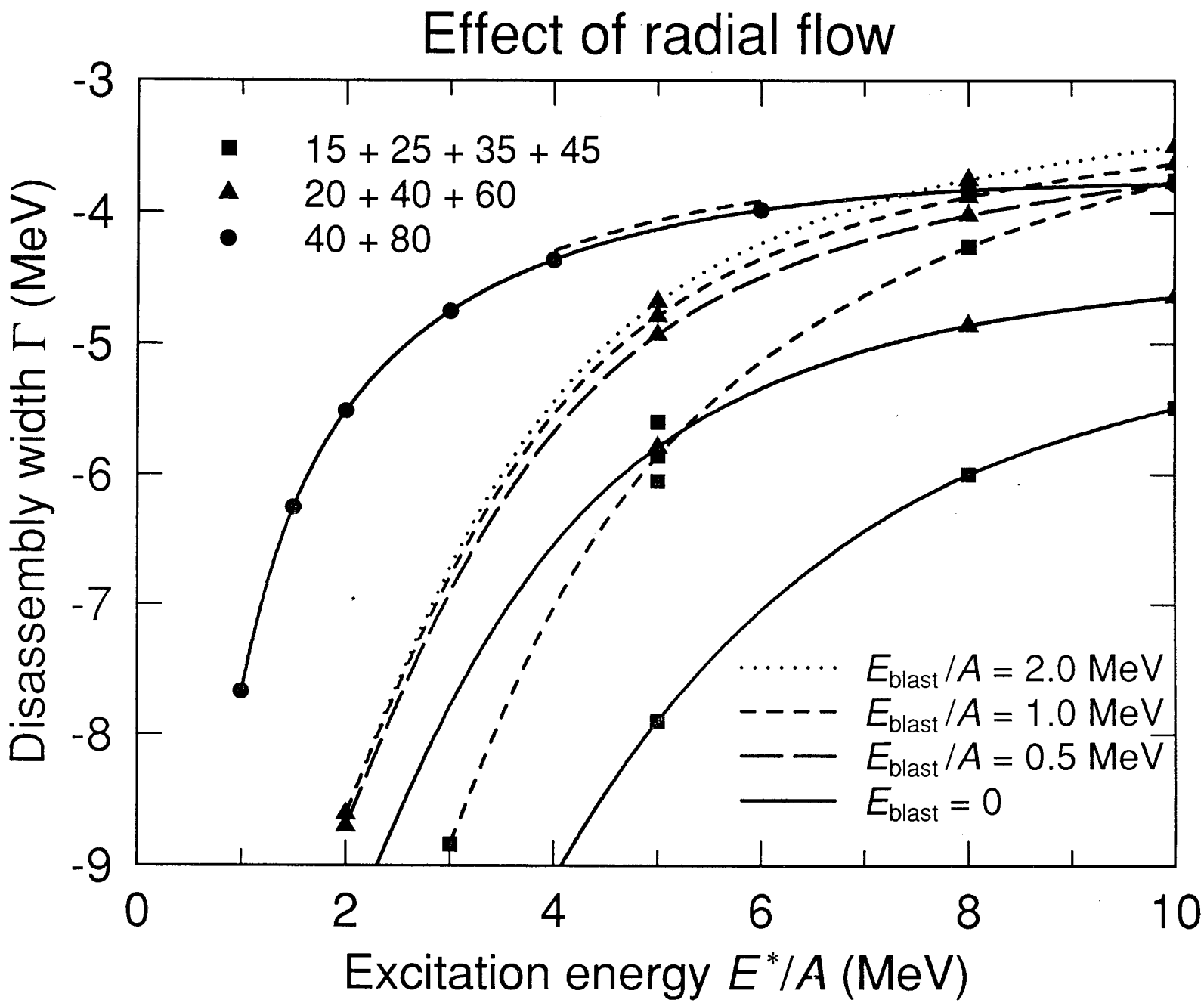
Effect of radial flow
15 + 25 + 35 + 45
20 + 40 + 60
40 + 80
E_{blast}/A = 2.0 MeV
E_{blast}/A = 1.0 MeV
E_{blast}/A = 0.5 MeV
E_{blast} = 0
Disassembly width Γ (MeV)
Excitation energy E^*/A (MeV)
-3
-4
-5
-6
-7
-8
-9
0
2
4
6
8
10

Figure 3

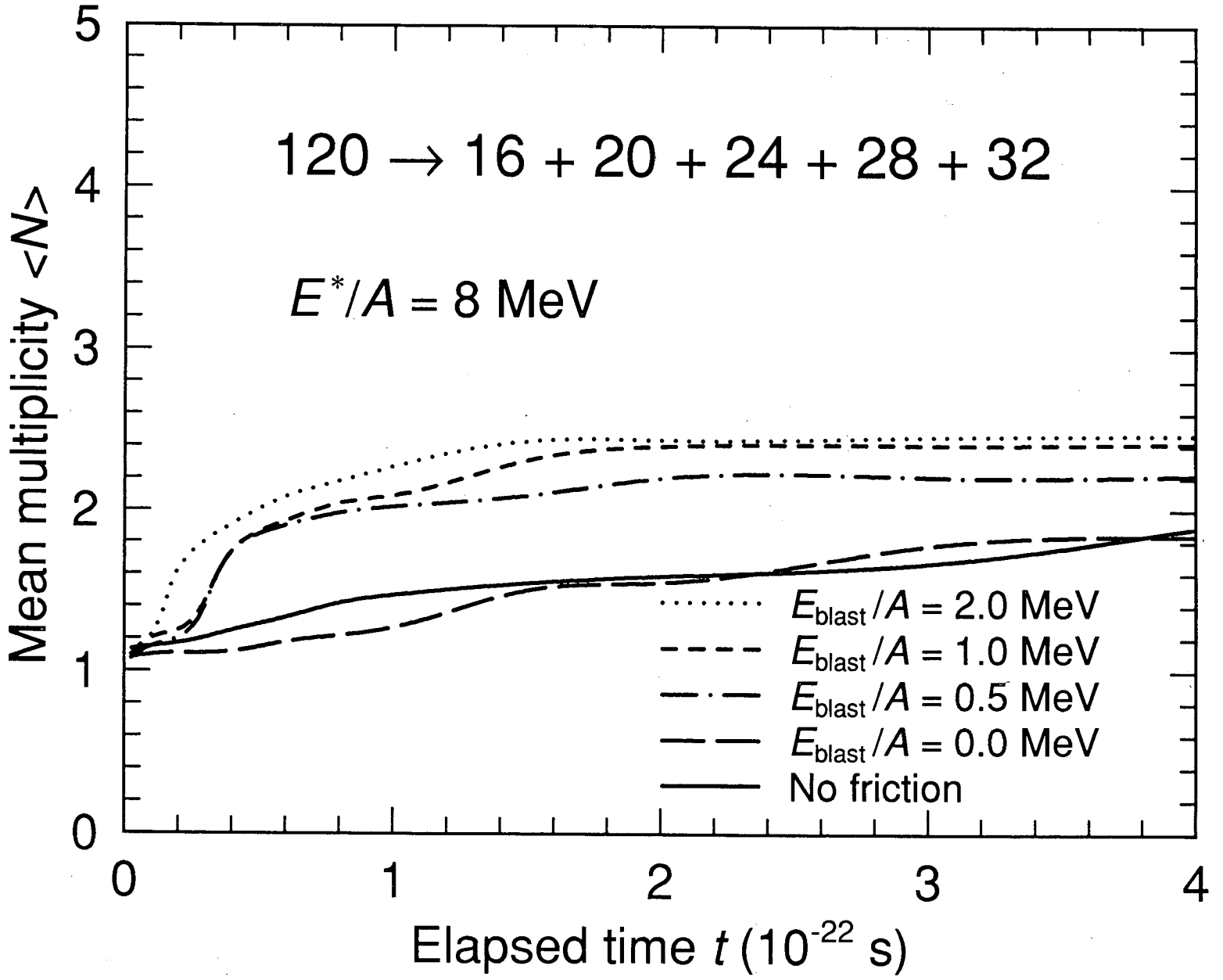
120 → 16 + 20 + 24 + 28 + 32
E*/A = 8 MeV
Mean multiplicity <N>
Elapsed time t (10^-22 s)
E_blast/A = 2.0 MeV
E_blast/A = 1.0 MeV
E_blast/A = 0.5 MeV
E_blast/A = 0.0 MeV
No friction
0
1
2
3
4
5

Figure 4

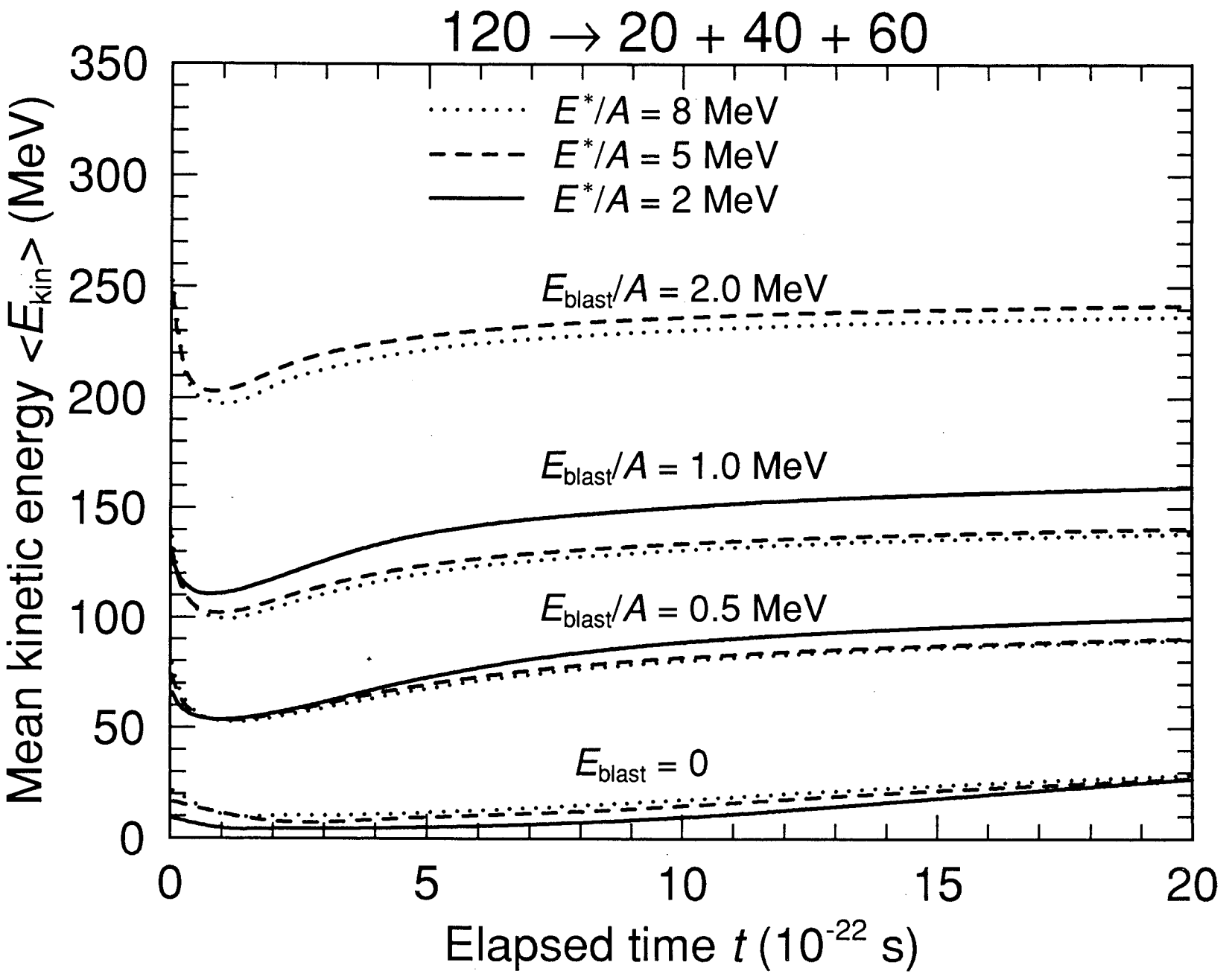
120 → 20 + 40 + 60
E*/A = 8 MeV
E*/A = 5 MeV
E*/A = 2 MeV
Eblast/A = 2.0 MeV
Eblast/A = 1.0 MeV
Eblast/A = 0.5 MeV
Eblast = 0
Mean kinetic energy <Ekin> (MeV)
Elapsed time t (10-22 s)
0
50
100
150
200
250
300
350
0
5
10
15
20

Figure 5

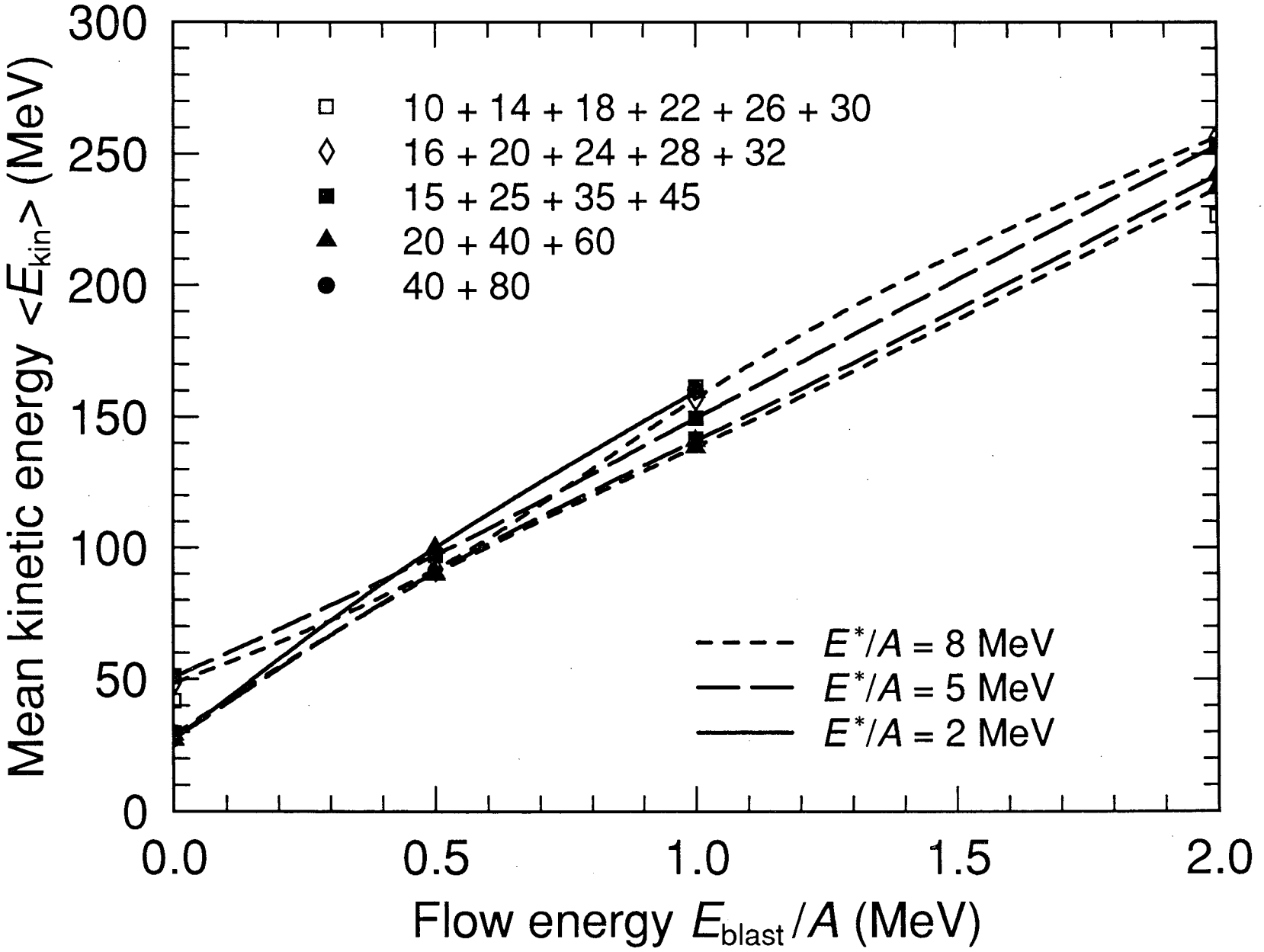
300
250
200
150
100
50
0
0.0
0.5
1.0
1.5
2.0
Mean kinetic energy <E_{kin}> (MeV)
Flow energy E_{blast}/A (MeV)
10 + 14 + 18 + 22 + 26 + 30
16 + 20 + 24 + 28 + 32
15 + 25 + 35 + 45
20 + 40 + 60
40 + 80
E^*/A = 8 MeV
E^*/A = 5 MeV
E^*/A = 2 MeV

Figure 6

LAWRENCE BERKELEY LABORATORY
TECHNICAL INFORMATION DEPARTMENT
1 CYCLOTRON ROAD
BERKELEY, CALIFORNIA 94720